Mon. Not. R. Astron. Soc. **000**, 1–4 (2012) Printed 23 June 2012 (MN LATEX style file v2.2)

# Origin of Interstellar Scintillations

Ue-Li Pen,[1⋆] Yuri Levin,[2]†

23 June 2012

**ABSTRACT**

We show that surface waves along aligned interstellar current sheets lead to pulsar scintillation properties consistent with those observed. It resolves several ISM challenges to explain the length scales and density scales required. In this picture, the interstellar medium is quiescent, with scintillation and scattering resulting from weak waves propagating along magnetic domain boundary current sheets, which are expected from helicity conservation. This model quantitatively predicts the spacing and amplitudes of inverted parabolic arcs. We present results for 1-D simulations. Multi-Frequency, multi-epoch VLBI observations can quantitatively test this picture. If successful, in addition to mapping the ISM, this opens the door to precise nanoarcsecond pulsar astrometry, distance measurements, and emission studies using these 100AU interferometers in the sky.

**Key words:** Interstellar Medium, reconnection, extreme scattering events

## 1 INTRODUCTION

The structure of the interstellar medium has remained enigmatic. Five decades of pulsar scintillation observationsScheuer (1968) have resulted in problematic physical requirements. Current observations have demonstrated that much of the scattering is dominated by a small number of very localized lensing screens(Brisken et al. 2010) along the line of sight. Within the lensing screen, the scattering is in turn dominated by spatially localized structures. This is difficult to understand with random diffractive processes in an extended turbulent medium.

## 2 TWO REGIMES OF LENSING: DIFFRACTIVE VS REFRACTIVE

Two regimes to generate pulsar scintillation have been considered. In the diffractive picture, the scattering/lensing angle is determined by the size of structure in the medium, compared to the wavelength $\lambda$: $\theta = 2\pi\lambda k$. The amplitude of each scattered structure is determined by the depth of the modulation. To explain the observed angles in the range $1 - 100$ mas at wavelength $\sim$ 1m, requires structures in the ISM on scales of order $10^{6-8}$m. This imposes unexpected properties on the interstellar medium, since it is much smaller than the coloumb mean free path of free electrons in the interstellar medium. In such mechanism, the angular image of a pulsar, and therefore its dynamic spectrum, are superpositions of many weak structures, and are expected to be roughly gaussian. The parabolically structured 2-D power spectrum of the dynamic spectrum, and the VLBI image of the scattering disk, are inconsistent with such a picture, at least for the long lag (ms) structures.

A second mechanism is due to refractive lensing. In this scenario, the bending angle is determined by Snell's law, i.e. the change in refractive index and the angles of incidence. The flux of the images is determined by the size of the lens over the impact parameter. This picture is also challenging to implement, since the observed scattering angles would naïvely require changes in free electron density of $\sim 10^3$, which are difficult to understand or confine.

Goldreich & Sridhar (2006) showed that refractive lensing results in scintillation similar to the diffractive picture. In this refractive lensing, localized refractive images act like a multiple slit interferometer. The beating of these images results in the rapid frequency and time variability, and has scalings very similar to the purely diffractive picture.

The discovery of parabolic arcs(Stinebring et al. 2001) and inverted arclets has required the existence of localized refractive lenses. Direct VLBI imaging of the scattering screen(Brisken et al. 2010) demonstrate the presence of discrete isolated lenses, i.e. scattering points, which are all in a single thin sheet. This leads to physical challenges of confining these lenses. Various solutions have been proposed(Walker 2007; Pen & King 2012; Goldreich & Sridhar 2006).

In this paper, we expand the picture of current sheets, and consider perturbations.

⋆ E-mail: pen@cita.utoronto.ca
† E-mail: yuri.levin@monash.edu

## 3 ASTROPHYSICAL PICTURE

The interstellar medium is stirred on scales of parsecs by various energetic processes, including supernovae, ionization fronts, spiral density waves, and other phenomena. These processes are generally short lived, and after the stirring, the warm medium relaxes to an equilibrium configuration. In the presence of helicity, the equilibrium magnetic fields are configured as interlaced twisted tori, which are long lived(Braithwaite & Spruit 2004). The magnetic fields are locally almost parallel, with discontinuous interface regions, a bit like magnetic domains in a ferromagnetGruzinov (2009).

At the boundary between between magnetic field configurations, current sheets maintain the discontinuities. These current sheets have been proposed to dominate the scattering of radio sources(Goldreich & Sridhar 2006).

## 4 SURFACE DYNAMICS

The current sheet is physically thin, $<\sim$ AU. On each side the magnetic field points in a different direction. The change in alvenic properties gives rise to surface wave(Jain & Roberts 1991; Joarder et al. 2009), which are analogous to deep water ocean waves. The restoring force is the difference in magnetic field component projected along the wave vector. Like ocean waves, these waves penetrate about a wavelength into each side. We will be considering wavelengths of thousands of AU, so the current sheet itself is neglible as far as the dynamics of the waves are concerned. Seen in projection along the aligned sheet, the projected wavelengths will be $\sim$ AU. The displacements are transverse to the wave vector, and perpendicular to the sheet. While alvenic in nature, the surface modes possess only one polarization, unlike bulk waves. These waves resemble a flag blowing in the wind. Disturbances travelling along the sheet are decoupled from bulk waves. Being confined to a sheet, the amplitude away from a source drops as $\propto 1/r$ instead of the normal inverse square law. A amplitude of order $\alpha\lambda$, or about $10^{-3}$ of the wavelength is sufficient to cause the sheet to appear folded in projection.

## 5 FOLD STATISTICS

Alven waves dissipate on scales shorter than the proton mean free path. We thus model the waves as a displacement function $\zeta(x)$ which is a Gaussian random field with a correlation function that is a Gaussian, $\xi(r) = \langle\zeta(x)\zeta(x+r)\rangle = \exp(-r^2/2/\sigma^2)$, where $\sigma$ is the dissipation scale. Figure 1 shows a realization of a sheet with a random fluctuations.

In projection, the surface density results in a highly non-Gaussian distribution. Figure 2 shows the density distribution in a simulation. Folds occur when the gradient of the displacement is equal to minus 1. The correlation function of the gradients is the second derivative of the displacements. The number of crossings of -1 depends on the variance of the gradient field. The density of the folded sheet is proportionate to the length of gradient spent in the vicinity of -1, which is turn is proportionate to the reciprocal of the derivative of the gradient. This second derivative is also a Gaussian random field. The second derivative is uncorrelated with the

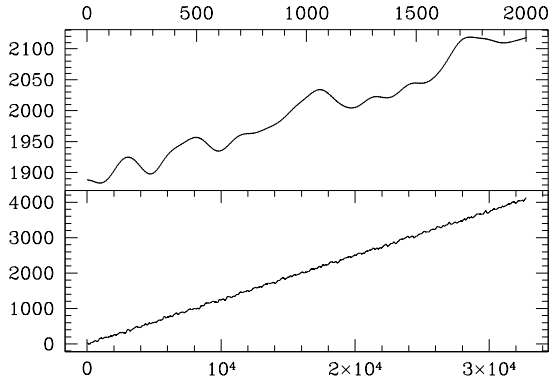


**Figure 1.** Sheet with transverse perturbations. The upper panel shows an zoomed version of a short section.

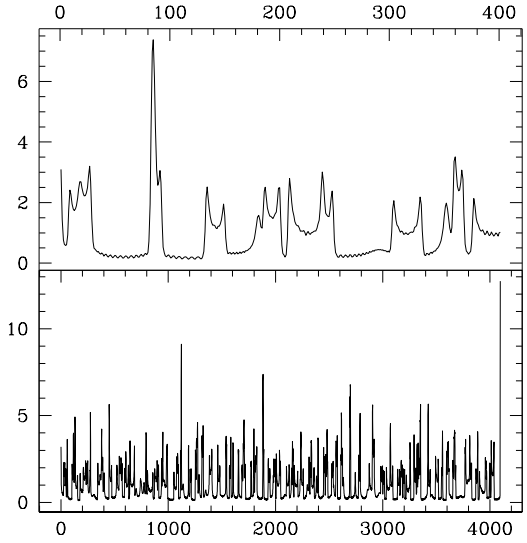


**Figure 2.** projected density. The upper panel is a zoom of the central portion of the lower panel. Each time the sheet folds in projection, we see a caustic structure in density.

first derivative. The one point PDF of the reciprocal of a Gaussian variable is

$$P(\rho) = \frac{\exp(-\frac{1}{2\rho^2})}{\sqrt{2\pi}\rho^2}. \quad (1)$$

This is a highly non-Gaussian distribution, and resembles a Lorenzian, with divergent moments. The very high tails are cut off by higher order derivatives of the correlation function.

These high density caustics give rise to refractive lensing processes which resemble the inverted parabolic arcs in pulsar secondary spectra.

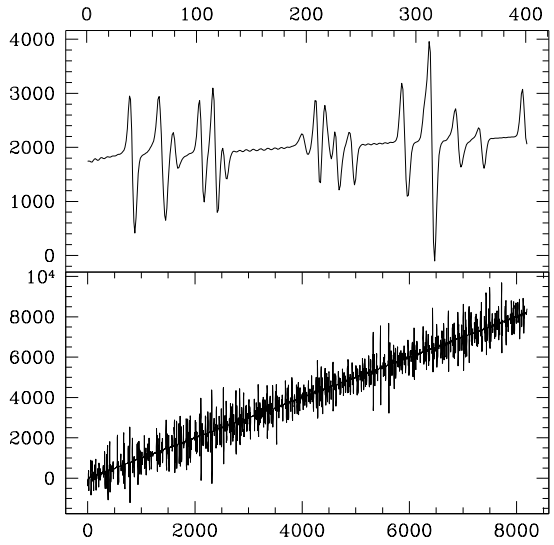


**Figure 3.** deflection angle mapping. The horizontal axis is angle on the sky, and the vertical axis is the intersection of this light ray on the source plane. Whenever multiple different directions on the sky intersect on the same position in the source plane, multiple images are formed, which form a coherent interference pattern.

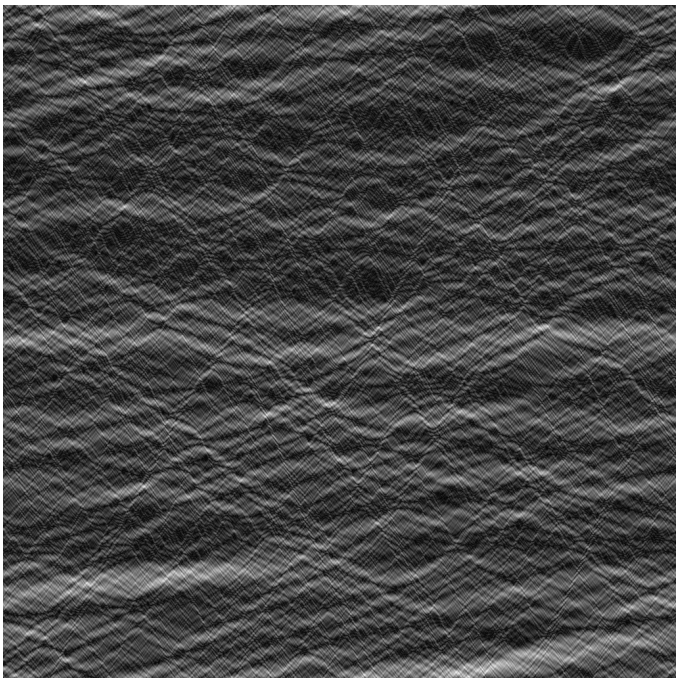

**Figure 4.** dynamic pulsar spectrum. Horizontal axis is time, vertical axis is frequency. We reproduce the characteristic criss-cross pattern observed in real scintillation spectra.

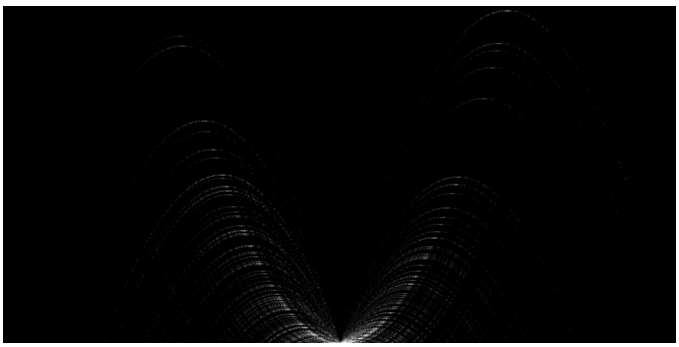

**Figure 5.** secondary pulsar spectrum. The inverted parabolic arcs arise naturally in this model.

## 6 LENSING

The lensing of this density sheet can be computed in analogy to Pen & King (2012).

Given the projected density distribution in Figure 2, we can compute the mapping of apparent angle on the sky to position in the source (pulsar) plane. The caustics in the projected density distribution lead to large angle deflections, and multiple imagine, whenever the sheets are aligned closer than the amplitude of the perturbations. This explains why only a small fraction of (edge-on) current sheets contribute to scintillation.

## 7 SIMULATED DYNAMIC SPECTRA

With the density field, we can solve the lens equations to simulate dynamic spectra. By adding the voltages on each image with their appropriate amplitude and phases, we simulate the dynamic spectrum, shown in figure 4.

A 2-D fourier transform maps this dynamic spectrum into a secondary spectrum, shown in figure 5.

We find that the interference of these discrete, co-linear images forms the inverted parabolic arcs that are observed.

## 8 DISCUSSION

We can estimate the length scales involved. This theory requires as input a current sheet thickness, inclination angle, curvature, amplitude of waves, and dissipation scale.

The thickness of the sheets is determined by the magnification of images: the flux is roughly the thickness divided by the impact parameter. It suggests a typical tickness of $h \sim 0.1$ AU. A wave of projected wavelength $\alpha\lambda$ enhances projected densities by a factor $w = \sqrt{h\alpha\lambda}$. The projected wavelengths are known to be of order $\sim 10$ AU, so $w \sim 10$. The largest deflection angles are $\gamma \sim 0.1$ mas, which requires a projected electron density change $\delta n_e/(w\alpha) \sim$. In an underdense sheet, the maximal change of density is the density itself. For the mean interstellar medium densities determined from pulsar dispersion, we obtain $\alpha \sim 10^{-2}$. The probability of seeing a sheet at such an angle is $\sim \alpha^2$, requiring the existence of $\sim 1/\alpha^2$ sheets along the line of sight. For B0834+06, the distance is $\sim$ 1 kpc, giving a typical sheet separation of $s \sim 0.1$ pc. If we assume the curvature to be separation (it could be smaller), we find a limiting projection angle $\alpha_{\rm min} = \sqrt{h/s} \sim 0.002$. The wave amplitudes must be $> \alpha\lambda$ in order to form projected caustics. This is a small amplitude, which rules out large amplitude universal turbulence. The latter would deform the sheet too much. In a Kolmogorov spectrum, the energy power spectrum scales as $k^{-5/3}$. Scaling from the alven damping scale to the fres-

nel scale, this results in density fluctuations $< 10^{-4}$. This is insufficient to create scintillation in pulsar fluxes.

These estimates are qualitative. One expects current sheets to come in a range of sizes, curvature and perturbation amplitude. The thickness might also vary, unless due to global resistivity.

## 9 CONCLUSIONS

We have presented a quantitative theory of pulsar scintillation inverse parabolic arcs. These extend recent ideas of thin current sheets, which naturally explain the large angle scattering observed in pulsars and some extragalactic sources.

This picture could explain all scintillation phenomena with structures greater than 0.1 AU. The apparent diffractive structure results from the interference between refractive images, and no diffractive scattering is needed.

## 10 ACKNOWLEDGEMENTS

U-LP thanks NSERC and CAASTRO for support.

## REFERENCES

Braithwaite J., Spruit H. C., 2004, Nat, 431, 819
Brisken W. F., Macquart J.-P., Gao J. J., Rickett B. J., Coles W. A., Deller A. T., Tingay S. J., West C. J., 2010, ApJ, 708, 232
Goldreich P., Sridhar S., 2006, ApJ, 640, L159
Gruzinov A., 2009, ArXiv e-prints
Jain R., Roberts B., 1991, Solar Physics, 133, 263
Joarder P. S., Ghosh S. K., Poria S., 2009, Geophysical and Astrophysical Fluid Dynamics, 103, 89
Pen U.-L., King L., 2012, MNRAS, 421, L132
Scheuer P. A. G., 1968, Nat, 218, 920
Stinebring D. R., McLaughlin M. A., Cordes J. M., Becker K. M., Goodman J. E. E., Kramer M. A., Sheckard J. L., Smith C. T., 2001, ApJ, 549, L97
Walker M. A., 2007, in Haverkorn M., Goss W. M., eds, SINS - Small Ionized and Neutral Structures in the Diffuse Interstellar Medium Vol. 365 of Astronomical Society of the Pacific Conference Series, Extreme Scattering Events: Insights into the Interstellar Medium on AU-Scales. p. 299